Energy and exergy analysis of a pilot plant for the combined production of cooling and electricity from a low temperature heat source through an absorption process

Simone Braccio, Alessia Arteconi, Hai Trieu Phan, Nicolas Tauveron, Nolwenn Le Pierrès

Energy and exergy analysis of a pilot plant for the combined production of cooling and electricity from a low temperature heat source through an absorption process.

Simone Braccio[a,e], Alessia Arteconi[b], Hai Trieu Phan[c], Nicolas Tauveron[d] and Nolwenn Le Pierrès[e]

[a]Univ. Grenoble Alpes, CEA, LITEN, DTCH. F-38000 Grenoble, France, simone.braccio@cea.fr, CA
[b]KU Leuven, Department of Mechanical Engineering, Geel, 2440, Belgium, alessia.arteconi@kuleuven.be
[c]Univ. Grenoble Alpes, CEA, LITEN, DTCH. F-38000 Grenoble, France, Haitrieu.PHAN@cea.fr
[d]Univ. Grenoble Alpes, CEA, LITEN, DTCH. F-38000 Grenoble, France, nicolas.tauveron@cea.fr
[e]LOCIE Laboratory, Université Savoie Mont Blanc CNRS UMR 5271, 73376 Le Bourget du Lac, France, nolwenn.le-pierres@univ-smb.fr

Abstract:

Research and development efforts are made worldwide in finding new, more efficient energy conversion technologies using renewable or recovery sources. In this context, absorption processes are well suited for the use of energy at low temperatures (80°C – 200°C) for the production of cooling and mechanical work.
The present work focuses on an innovative cold and electricity combined production system based on an ammonia-water absorption chiller coupled to an axial turbine. The study is based on an experimental pilot plant of 10 kW thermal power input at the ammonia vapour desorber, to which the integration of a partial admission turbo-expander for the production of mechanical work is under investigation.
A 1D model of the turbine validated on CFD simulations is integrated in a validated model of the absorption machine and used to conduct an analysis of the interactions between the turbine and the cycle that contains it. The constraints imposed by the expander (vapour quality, relationship between flowrate and pressure) are highlighted and the use of a throttling process is evaluated as a way to add flexibility. A parametric analysis is performed changing the operating conditions to investigate the energy performance of the cycle. Subsequently, an exergy analysis is undertaken, for both the simple absorption and combined cycle configuration, to identify the components where most of the exergy destruction takes place and to find the hot source temperature maximizing exergy efficiency for fixed operating conditions. The results obtained provide reliable insights on the integration of this type of expander in an absorption cycle.

Keywords:

Absorption chiller; Ammonia/water; Combined cooling and power; Exergy.

1. Introduction

Ever-increasing global demand for energy in a context of scarce fossil resources and the need of cutting greenhouse gas emissions are driving research efforts towards the development of increasingly efficient conversion technologies. This interest involves all sectors and in particular the production of cooling and electricity, whose demand is expected to triple between 2016 and 2050 [1]. In these circumstances, the use of renewable or recovery low temperature heat sources has become a priority. To that end, the most relevant thermodynamic cycles are [2]: three temperatures cycles involving liquid/gas or solid/gas sorption processes for the production of cooling, and Organic Rankine Cycles (ORC) for the production of electricity. Thermochemical sorption processes are intrinsically discontinuous while absorption cycles are characterized by a continuous cold (or heat) production and by good Coefficients Of Performance (COP) from 0.6 to 1. ORCs allow tailoring of the cycle to the heat source thanks to an appropriate selection of the working fluid, thus providing an efficient mechanical energy production. Absorption and Rankine cycles share various components necessary to the phase changes of the working fluid. Thus, their coupling seems promising, since it could lead to an increased overall efficiency of the system as well as to the mutualisation of some components [3]. A first overview of these systems was proposed by Ayou et al.[4], who identified two main architectures of combined cooling and power (CCP) cycles: in series and in parallel architectures. The former ones are generally more efficient for the production of power, while the latter ones offer more flexibility.

This work focuses on a parallel cooling and electricity production system using a low temperature heat source. The study is based on an experimental prototype of ammonia-water absorption chiller [5] to which a turbine is being integrated for power production. Ammonia-water is one of the most common working pair used in CCP cycles, since temperature and pressure of the ammonia vapour at the desorber outlet are sufficient to produce mechanical power. Despite its toxicity for humans, advantages of this pair include no crystallisation, compactness, no environmental harm and possibility of working at sub-zero temperatures. The technology selected for the production of power, an axial impulse turbine, limits the leaking losses and excessively small dimension, thus guarantying a good level of mechanical work output even at the small prototype scale. Nevertheless, the functioning of the expander imposes several constraints on the cycle. Attention has to be paid to the interconnections between the physics governing the turbine and the cycle that integrates it. The energy and exergy methods were applied to evaluate the efficiency of the proposed combined cycle. Exergy parameters such as fuel, products, lost and destroyed exergy as well as exergy efficiencies were calculated. The analyses developed show the potential of the cycle to produce both power and cooling, even at small lab scale.

2. Methods

2.1. Cycle description

The CCP cycle under investigation, is schematically shown Fig. 1. The functioning is based on an ammonia-water absorption machine with an expander coupled in parallel to the cold production line. The liquid solution rich in ammonia at the absorber outlet is pumped into the desorber where a supply of heat $\dot{Q}_d$ from the hot source allows the partial desorption of the ammonia vapour. The desorber integrated in the cycle is a recently developed component, which operates an internal rectification of vapour with the entering solution in order to eliminate the remaining traces of water, detrimental for the good functioning of the system. The poor solution preheats the rich solution in the solution heat exchanger and is then expanded before returning to the absorber. The refrigerant vapour produced at the desorber is divided between the cold and electricity production lines.

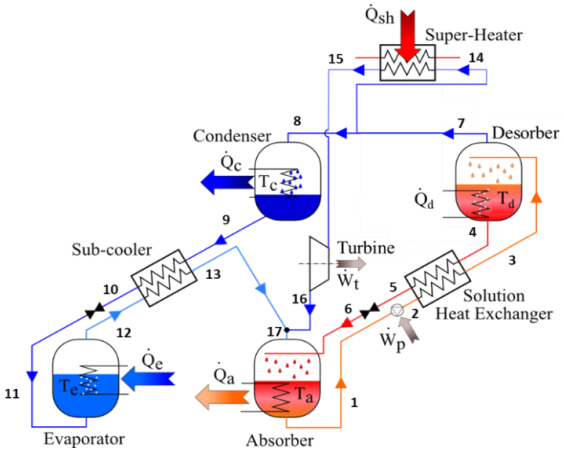

Fig. 1. Scheme of the combined cycle

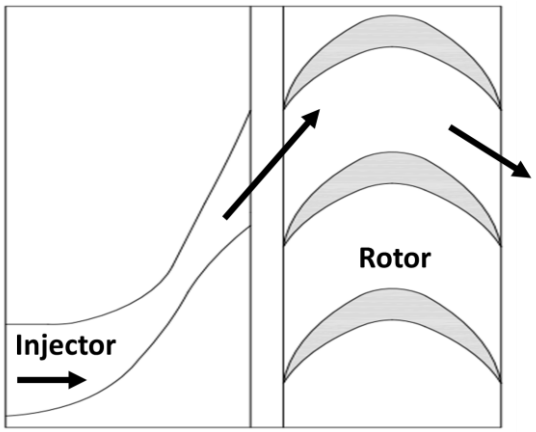

Fig. 2. Scheme of the turbine

On the cold production side, ammonia is condensed through the exchange of the thermal power $\dot{Q}_c$ with an intermediate temperature source. The liquid refrigerant is expanded in a valve to reach the low pressure before cooling the cold source at the evaporator by absorbing the power $\dot{Q}_e$. A subcooler is used to precool the ammonia before the expansion by using the flow coming out of the evaporator.

On the electricity production side, a superheater provides the power $\dot{Q}_{sh}$ to increase the temperature of the vapour to avoid its condensation during the expansion in the turbine for the production of the mechanical power $\dot{W}_t$. The expander selected and considered in the present study (Fig. 2), is a partial admission supersonic axial turbine, with a single converging-diverging injector where all the expansion takes place. Taking into account the very low steam mass flow rate available, a partial admission machine helps to avoid excessively small dimensions or high rotational speeds. In addition, the choice of an axial turbine allows the extrapolation of results obtained to larger plant sizes.

The flows of the cold and electricity production lines mix (point 17). They are absorbed in the poor solution thanks to the cooling by an intermediate temperature source (usually the same as the condenser), to which the power $\dot{Q}_a$ is transferred. Table 1 shows the nominal operating points of the components of the pilot plant on which the study is based. The temperatures indicated refer to the Heat Transfer Fluid (HTF) side, with which the working mixture exchanges heat.

Table 1. Nominal operating point of the components of the pilot plant.

Nominal Values	Evaporator	Condenser	Absorber	Desorber
HTF Temperature [°C]	18/13	27/32	27/32	95/90
Pressure [bar]	6	12	6	12
Power [kW]	7	7	9	10

2.2. Cycle model

A numerical model of the absorption cycle was developed in EES (Engineering Equation Solver). The correlations proposed by Ibrahim and Klein [6] were selected to calculate the thermodynamic properties of the ammonia-water mixture because of their good agreement with experimental data. Energy and mass balances are formulated for each component under the steady state assumption. Since the inertia of the components are large and thanks to their continuous functioning, the assumption is indeed experimentally verified. The mixture is considered to be at saturation at the outlet of the absorber, desorber and condenser and at the inlet of the evaporator. It follows that the condenser outlet temperature defines the high pressure of the cycle, while the evaporator inlet temperature defines its low pressure. Additionally the isentropic efficiency of the pump was considered equal to 80% [5], resulting in a neglectable power (around 30 W) absorbed by the pump in the nominal point. Pressure drops and heat losses were also neglected. Exchangers are characterised through semi-empirical efficiencies developed for each component based on experimental data using three dimensionless operating parameters: the number of transfer units, the energetic ratio and the Jakob number. The results of the model, detailed in [7], were tuned on experimental results of the pilot plant. Results show the same tendencies and very good agreement with experimental measures, with a maximum error in low efficiency off-design points below 6% and 15% for the predicted COP and cooling power output respectively.
To complete the development of the combined cycle, a compressible 1D model of the turbine was developed and integrated in the absorption chiller model. The use of a simplified loss model, described in [8], allows to estimate the performance of the turbine also in off-design conditions. The coefficients of the loss model have been adjusted based on CFD simulations of the turbine produced for the pilot plant.
For the purpose of evaluating the efficiency of cooling production of the cycle, the thermal COP of the cooling production is defined as follows:

$$COP_R = \frac{\dot{Q}_e}{\dot{Q}_d \cdot r_s} . \quad (1)$$

To account for the fact that not all the refrigerant vapour is used for the cooling production, $\dot{Q}_d$ is multiplied by the split ratio r_s of the mass flow rate passing through the evaporator to the vapour mass flow rate produced at the desorber:

$$r_s = \frac{\dot{m}_{11}}{\dot{m}_7} . \quad (2)$$

On the other hand, the efficiency of the power cycle is calculated as follows:

$$\eta_{power} = \frac{W_t}{\dot{Q}_d \cdot (1 - r_s) + \dot{Q}_{sh}} . \quad (3)$$

One can then define an overall energy efficiency (η_e) of the cycle [9] defined as the average weighted on r_s of COP_R and η_{power}

$$\eta_e = COP_R \cdot r_s + \eta_{power} \cdot (1 - r_s) . \quad (4)$$

It is also possible to compare this parameter with and ideal coefficient of performance defined as:

$$\eta_{e,id} = COP_{carnot} \cdot r_s + \eta_{carnot} \cdot (1 - r_s) \quad (5)$$

Where COP_{carnot} and η_{carnot} are respectively the Carnot coefficient of performance of cold production and the Carnot efficiency of power production defined as:

$$COP_{carnot} = \frac{T_d - T_a}{T_d} \cdot \frac{T_e}{T_a - T_e} . \quad (6)$$

$$\eta_{carnot} = \frac{T_{sh} - T_a}{T_{sh}} . \quad (7)$$

It is important to notice that since η_e and $\eta_{e,id}$ treat power and cooling output as additive properties, they represent a measure of the energy efficiency of the cycle. The exergetic efficiency of the cycle could be expressed as:

$$\eta_{ex} = \frac{COP_R}{COP_{carnot}} \cdot r_s + \frac{\eta_{power}}{\eta_{carnot}} \cdot (1 - r_s) . \quad (8)$$

The expression of Eq. (8) approximates well the exergetic efficiency of the system described by Eq. (11) and the two coincide when the temperature of the heat source is constant.

2.3. Exergy analysis

The energy analysis method is widely used to evaluate thermodynamic systems. However, this method is only concerned with energy conservation and may not be sufficient to investigate the performance of a system. The method of exergy analysis provides insights that enable the identification of the irreversibilities occurring in a system as well as the evaluation of their magnitude.

Exergy is the maximum theoretical useful work obtainable from a system of interest interacting to equilibrium with an idealized system called environment, defined by T_0 and P_0, here considered of 25 °C and 1.013 bar respectively. Exergy is not generally conserved and can be destroyed as thermodynamic irreversibilities reduce the exergy of a system. Considering a steady state control volume, the exergy balance states that the rate at which exergy is transferred into the control volume must exceed the rate at which exergy is transferred out, the difference being the destroyed exergy $\dot{E}x_D$:

$$\sum_j(\dot{E}x_{i,j} + \dot{E}x_{Q,i,j}) = \sum_j(\dot{E}x_{o,j} + \dot{E}x_{Q,o,j}) + \dot{W}_{cv} + \dot{E}x_D \,. \tag{9}$$

$\dot{E}x_{Q,j}$ is the thermal exergy, associated to heat transfer out or into the control volume and defined as:

$$\dot{E}x_{Q,j} = \left(1 - \frac{T_0}{T_j}\right) \cdot \dot{Q}_j \,. \tag{10}$$

$\dot{W}_{cv}$ represents the rate of energy transfer of work other than flow work and $\dot{E}x_{in}$ and $\dot{E}x_{out}$ are exergy transfer rates at inlet and outlet. In the absence of nuclear, magnetic, electrical and surface tension effects, they can be divided into four components [10]: physical exergy Ex^{PH}, chemical exergy Ex^{CH}, kinetic exergy Ex^{KN} and potential exergy Ex^{PT}. Kinetic and potential exergy are usually neglected [11] and therefore the total exergy of a stream becomes the sum of physical and chemical exergy [12]:

$$\dot{E}x = \dot{m} \cdot ex = \dot{E}x^{PH} + \dot{E}x^{CH} \,. \tag{11}$$

The physical exergy is associated to the temperature and pressure of a stream of matter and is given by the following expression:

$$\dot{E}x^{PH} = \dot{m} \cdot ex^{PH} = \dot{m} \cdot [\,(h - h_0) - T_0 \cdot (s - s_0)] \,. \tag{12}$$

Physical exergy does not take into account the exergy component associated to the departure of the chemical composition of a system from that of the environment, which can be evaluated through chemical exergy. The calculation of chemical exergy based on standard chemical exergy values of respective species is detailed, among others, by Bejan et al. [10] and Szargut et al. [13].For the combined ammonia-water cycle considered, the chemical exergy of the flows is calculated using the following relation:

$$\dot{E}x^{CH} = \dot{m} \cdot ex^{CH} = \dot{m} \cdot \left[\left(\frac{x}{M_{NH_3}}\right) \cdot e^0_{NH_{3,CH}} + \left(\frac{1-x}{M_{H_2O}}\right) \cdot e^0_{H_2O,CH}\right] . \tag{13}$$

Where x is the ammonia mass fraction, while $e^0_{NH_{3,Ch}}$ and $e^0_{H_2O,Ch}$ are the standard chemical exergy of ammonia and water respectively, and their values are taken from Szargut et al. [13].

As exergy gives information about the quality of energy, the exergetic efficiency provides a true measure of the performance of a system. In order to define this parameter, it is necessary to identify both a product and a fuel of the system studied. The product is the desired useful effect, while the fuel represents the resources spent to generate the product. An exergy rate balance for the system can be then written as:

$$\dot{E}x_F = \dot{E}x_P + \dot{E}x_L + \dot{E}x_D \,. \tag{14}$$

where $\dot{E}x_F$ is the fuel exergy, $\dot{E}x_P$ is the product exergy, $\dot{E}x_L$ is the exergy loss (the exergy associated with the heat rejected to the environment) and $\dot{E}x_D$ is the exergy destroyed. The exergetic efficiency is the ratio between the product and fuel exergy:

$$\eta_{ex} = \frac{\dot{E}x_P}{\dot{E}x_F} \,. \tag{15}$$

Fig. 3 shows the exergy streams entering and exiting the system, the net exergy flow on each heat exchanger being the difference between the HTF exergy at inlet and at outlet. It is then possible to define the fuel, product and lost exergy of the cycle under investigation, as shown in Table 2.

In order to evaluate the exergy destroyed in each component, Equation (9) can be applied to all the cycle elements subsystems. On the other hand, the definition of a product and the calculation of an exergetic efficiency is not immediate for all components when considering them individually (Table 3). For example, this is the case of throttling valves, exchangers crossing T_0(usually the case of the subcooler in this cycle) or cooling heat exchangers, like the condenser, that serve other components. In addition, a comparison of exergetic efficiencies of dissimilar devices is generally not meaningful [10].

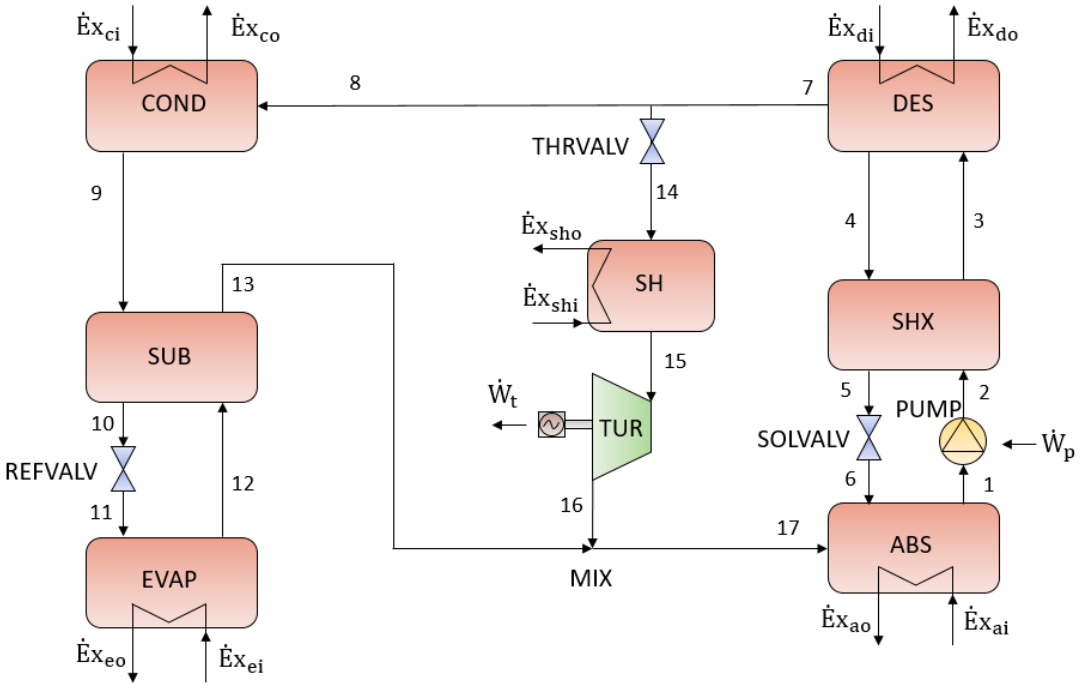

Fig. 3. Exergy streams in the system.

Table 2. Fuel and product definition for the overall system.

Overall System	
Exergy fuel	$\dot{E}x_{\mathrm{F}} = \dot{E}x_{di} - \dot{E}x_{\mathrm{do}} + \dot{E}x_{shi} - \dot{E}x_{\mathrm{sho}} + \dot{W}_{\mathrm{p}}$
Exergy product	$\dot{E}x_{\mathrm{P}} = \dot{W}_{\mathrm{t}} + \dot{E}x_{ei} - \dot{E}x_{eo}$
Exergy losses	$\dot{E}x_{\mathrm{P}} = \dot{E}x_{co} - \dot{E}x_{ci} + \dot{E}x_{\mathrm{ao}} - \dot{E}x_{\mathrm{ai}}$

Table 3. Fuel, product and loss definition for the overall system.

Component	Fuel	Product	Loss
Absorber	$\dot{E}x_{\mathrm{F,a}} = \dot{E}x_{17} + \dot{E}x_{6} - \dot{E}x_{9}$	−	$\dot{E}x_{\mathrm{L,a}} = \dot{E}x_{\mathrm{ao}} - \dot{E}x_{\mathrm{ai}}$
Condenser	$\dot{E}x_{\mathrm{F,c}} = \dot{E}x_{8} - \dot{E}x_{9}$	−	$\dot{E}x_{\mathrm{L,c}} = \dot{E}x_{\mathrm{co}} - \dot{E}x_{\mathrm{ci}}$
Desorber	$\dot{E}x_{\mathrm{F,d}} = \dot{E}x_{di} - \dot{E}x_{\mathrm{do}}$	$\dot{E}x_{\mathrm{P,d}} = \dot{E}x_{7} + \dot{E}x_{4} - \dot{E}x_{3}$	−
Evaporator	$\dot{E}x_{\mathrm{F,e}} = \dot{E}x_{11} - \dot{E}x_{12}$	$\dot{E}x_{\mathrm{P,e}} = \dot{E}x_{\mathrm{eo}} - \dot{E}x_{\mathrm{ei}}$	−
Pump	$\dot{E}x_{\mathrm{F,p}} = \dot{W}_{\mathrm{p}}$	$\dot{E}x_{\mathrm{P,p}} = \dot{E}x_{2} - \dot{E}x_{1}$	−
Refrigerant expansion valve	$\dot{E}x_{\mathrm{F,refvalv}} = \dot{E}x_{10} - \dot{E}x_{11}$	−	−
Solution expansion valve	$\dot{E}x_{\mathrm{F,solvalv}} = \dot{E}x_{5} - \dot{E}x_{6}$	−	−
Solution heat exchanger	$\dot{E}x_{\mathrm{F,shx}} = \dot{E}x_{4} - \dot{E}x_{5}$	$\dot{E}x_{\mathrm{P,shx}} = \dot{E}x_{3} - \dot{E}x_{2}$	−
Subcooler	$\dot{E}x_{\mathrm{F,sub}} = \dot{E}x_{9} - \dot{E}x_{10}$	$\dot{E}x_{\mathrm{P,sub}} = \dot{E}x_{13} - \dot{E}x_{12}$	−
Superheater	$\dot{E}x_{\mathrm{F,sh}} = \dot{E}x_{shi} - \dot{E}x_{\mathrm{sho}}$	$\dot{E}x_{\mathrm{P,sh}} = \dot{E}x_{15} - \dot{E}x_{14}$	−
Turbine	$\dot{E}x_{\mathrm{F,t}} = \dot{E}x_{15} - \dot{E}x_{16}$	$\dot{E}x_{\mathrm{P,t}} = \dot{W}_{t}$	−

However, knowing the values of exergy destroyed ($\dot{E}x_{D,k}$) and exergy loss ($\dot{E}x_{L,k}$) in each component, it is interesting to calculate the ratio of exergy destruction and exergy loss ratios, expressed as follows:

$$Y_{D,k} = \frac{\dot{E}x_{D,k}}{\dot{E}x_{F}}, \tag{16}$$

$$Y^{*}_{D,k} = \frac{\dot{E}x_{D,k}}{\dot{E}x_{D}}, \tag{17}$$

$$Y_{L,k} = \frac{\dot{E}x_{L,k}}{\dot{E}x_{F}}. \tag{18}$$

3. Results and discussion

3.1. Energy analysis

The integration of the turbine model in the adjusted absorption cycle model allows evaluating the performance of the combined cooling and power plant. Table 4 shows the effect of integrating the turbine into the cycle at the nominal operating point characterised by a pump mass flow rate of 100 kg/h, hot source temperature of 95 °C, an intermediate source temperature of 27 °C and a cold source temperature of 18 °C.

Table 4. Effect of the turbine on the cycle at nominal operating conditions.

	$\dot{Q}_e$ [kW]	$\dot{W}_{turb}$ [kW]	$\dot{m}_8$ [kg/h]	$\dot{m}_{14}$ [kg/h]	$\dot{Q}_d$ [kW]	$\dot{Q}_{sh}$ [kW]	COP_c [-]	η_{power} [-]	$\eta_{is,turb}$ [-]
Turbine line closed	6.75	-	24.54	-	9.83	-	0.68	-	-
Turbine line open	5.19	0.13	16.24	17.64	13.88	0.68	0.75	0.017	0.22

When the turbine line is open, the vapour mass flow rate produced at the desorber is divided between the power and cooling production lines. Since a lower mass flow rate passes through the exchangers of the cooling part of the cycle, their efficiency increases and therefore the overall cycle efficiency, resulting in a higher mass flow rate of vapour circulating in the system. A parametric analysis on the temperature of the sources was performed around the nominal operating point in order to better characterise the behaviour of the machine.

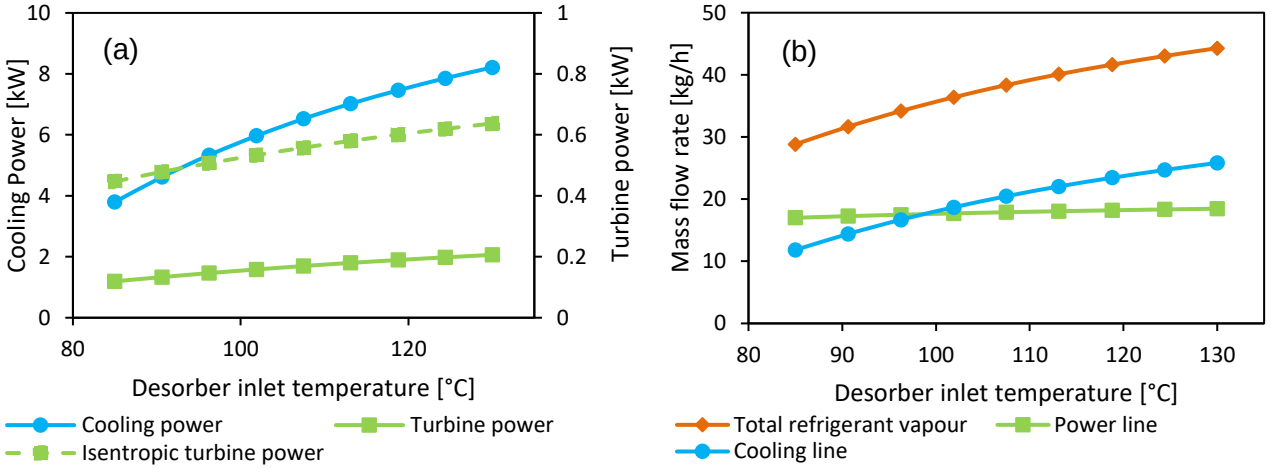

Fig. 4. Impact of the desorber inlet temperature on (a) the output of the system and (b) on the refrigerant vapour mass flow rate.

As an example, Fig. 4 shows the impact of increasing the desorber inlet temperature on the performance of the cycle. The losses linked to the small size and to the partial admission of the turbine highly penalize the power production of the cycle. Thus, it is interesting to look also at the power that could be produced by an isentropic turbine (dotted line in Fig. 4 (a)) as an upper performance limit. A higher hot source temperature increases the power exchanged at the desorber for a fixed solution mass flow rate, and thus the refrigerant vapour mass flow rate produced (Fig. 4 (b)). This increases considerably the cooling power output (Fig. 4 (a)), but moderately increases the mechanical power output. In fact, the mass flow rate treated by the turbine only slightly increases, passing from 17 kg/h at 85 °C to 18.4 kg/h at 130 °C, because of the high pressure increase (from 11.4 to 12.4 bar) due to the higher pinch on the condenser caused by the hotter vapour.

This highlights the strict limits that this type of expander imposes to the cycle, both in terms of the vapour inlet conditions needed to avoid condensation during the expansion, which requires the presence of a superheater, and in terms of mass flow rate treated. Particularly, the latter constraint restrains the flexibility of the cycle, making it impossible to regulate the ratio of cooling and power production according to the actual needs for fixed sources temperatures.

The introduction of a throttling valve before the turbine can add a degree of freedom to the system, allowing to reduce the pressure upstream of the turbine at the cost of a reduction of the overall efficiency. This possibility was evaluated through the addition of an adjustable adiabatic throttling process before the superheater. A throttling ratio was then defined as the downstream over the upstream pressure to the valve:

$$R_{th} = \frac{P_{14}}{P_7}. \quad (19)$$

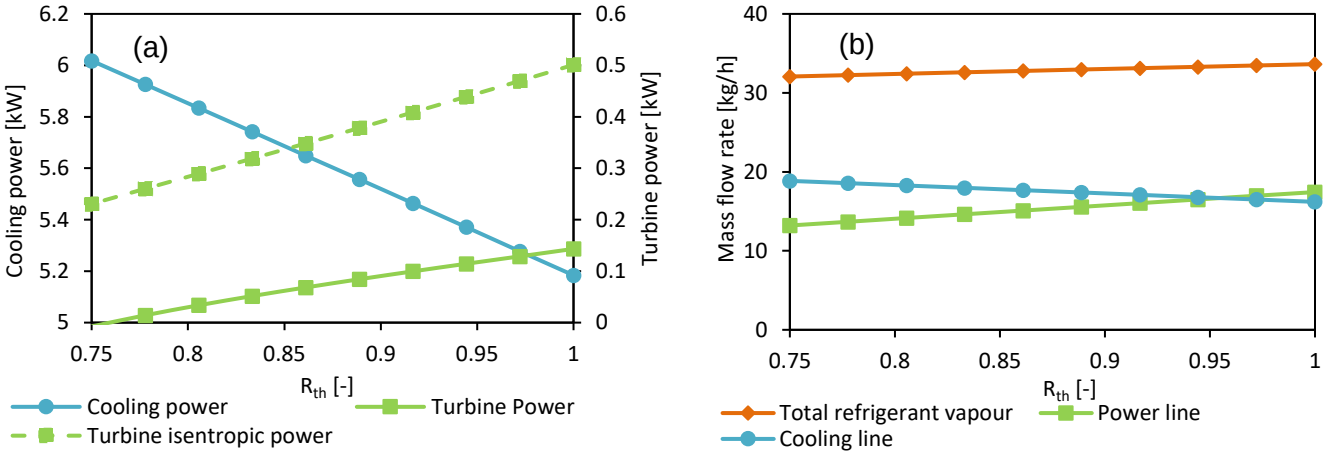

Fig. 5. Impact of a throttling process before the turbine.

Fig. 5(b), referring to the nominal operating point, shows that a throttling process allows reducing the mass flow rate treated by the turbine and increasing the mass flow rate in the cooling line of the machine. Reducing the turbine inlet pressure of around 25% ($R_{th} \approx 0.75$) allows increasing the cooling power from 5 kW to 6 kW. Nevertheless, for this value of pressure, the power production of the turbine goes to zero, Fig. 5(a), due both to the reduced enthalpy drop available and to the reduction of the turbine efficiency.

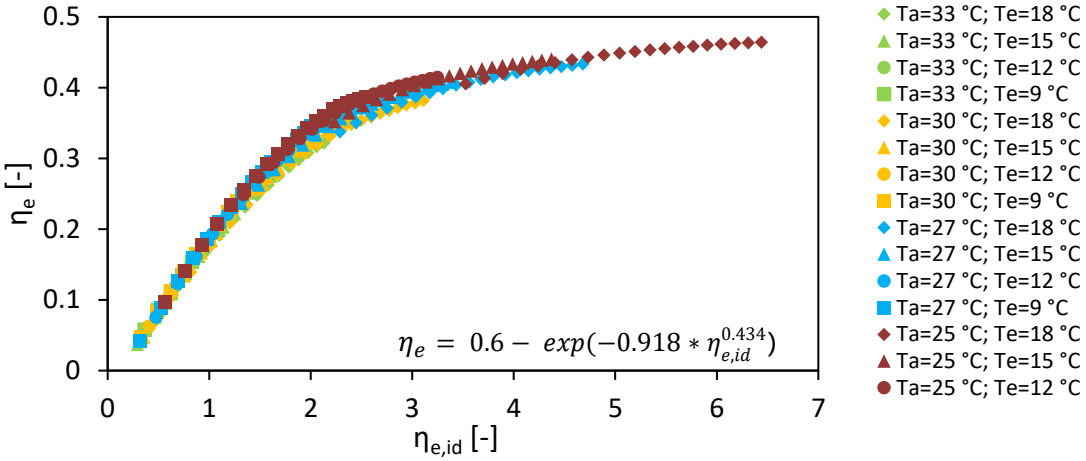

Fig. 6. Overall (η_e) vs ideal overall energy efficiency ($\eta_{e,id}$) map of the pilot plant.

Similar considerations apply also for variation of the cold and intermediate source temperatures. Lowering the cold source temperature decreases the low pressure of the cycle and therefore the efficiency of the absorption process, thus reducing the COP_c and the vapour mass flow rate. The turbine mass flow rate remaining constant, it is the mass flow rate in the cold production line that is reduced. This cold production flow rate approaches zero for a cold source temperature around 8°C (for other conditions fixed at nominal point). While reducing the evaporator temperature has a negative impact on the cooling production of the cycle, it improves the performance of the power production side thanks to the higher pressure drop available.

The effect of the condenser inlet temperature is opposite, as its rise increases the high pressure of the cycle. Therefore, a larger pressure drop is available to the turbine, increasing its power output and the efficiency. On the other hand, increasing the pressure of the cycle reduces the circulating mass flow rate of refrigerant vapour. The cold ratio r_c (Eq. (2)) approaches zero for condenser inlet temperatures increasing from the nominal point to around 33°C. Fig. 6 shows a mapping of the energy performance of the machine, measured by η_e versus $\eta_{e,id}$. It was obtained by variating T_d between 85-125 °C, T_a between 25-33 °C and T_e between 9-8 °C. It can be noted that the η_e initially increases when the $\eta_{e,id}$ increases, but tends towards an asymptote for higher values of $\eta_{e,id}$. The asymptotic value of η_e, determined by the design of the machine, corresponds to the maximum output that can be produced by the machine and is in line with the maximum performance reported by absorption machines constructors [14].

3.2. Exergy analysis

The exergetic performance of the system is evaluated at nominal operating conditions. Tables A1 and A2 presents the calculated thermodynamic properties at the various points of the ammonia-water cycle for the simple absorption and CCP configuration. The main exergetic quantities are given in Table 5 and Table 6.

Table 5. Exergy balance table for the simple absorption configuration at nominal operating conditions.

Component	$\dot{E}x_{F,k}$ $[kW]$	$\dot{E}x_{P,k}$ $[kW]$	$\dot{E}x_{Dk}$ $[kW]$	$\dot{E}x_{Lk}$ $[kW]$	$Y_{D,k}$ $[-]$	$Y^*_{D,k}$ $[-]$	$Y_{L,k}$ $[-]$	$\eta_{ex,k}$ [%]
Absorber	-	-	0.528	0.152	0.287	0.394	0.083	-
Condenser	-	-	0.173	0.121	0.094	0.281	0.065	-
Desorber	1.812	1.436	0.376	-	0.204	0.129	-	79%
Evaporator	-	-	0.081	-	0.044	0.060	-	73%
Refrigerant valve	-	-	0.007	-	0.003	0.005	-	-
Solution valve	-	-	0.014	-	0.007	0.010	-	-
Pump	0.025	0.02	0.004	-	0.002	0.003	-	80%
Solution heat exchanger	0.488	0.34	0.148	-	0.080	0.110	-	69%
Subcooler	0.2942	0.2895	0.004	-	0.002	0.003	-	-

Table 6. Exergy balance table for the CCP cycle configuration at nominal operating conditions.

Component	$\dot{E}x_{F,k}$ $[kW]$	$\dot{E}x_{P,k}$ $[kW]$	$\dot{E}x_{Dk}$ $[kW]$	$\dot{E}x_{Lk}$ $[kW]$	$Y_{D,k}$ $[-]$	$Y^*_{D,k}$ $[-]$	$Y_{L,k}$ $[-]$	$\eta_{ex,k}$ [%]
Absorber	-	-	0.615	0.313	0.228	0.307	0.1163	-
Condenser	-	-	0.096	0.076	0.036	0.048	0.0359	-
Desorber	2.508	1.832	0.675	-	0.250	0.338	-	73%
Evaporator	-	-	0.056	-	0.020	0.028	-	74%
Mixing	-	-	0.044	-	0.016	0.022	-	-
Refrigerant valve	-	-	0.005	-	0.002	0.002	-	-
Solution valve	-	-	0.011	-	0.004	0.006	-	-
Pump	0.036	0.019	0.017	-	0.006	0.008	-	80%
Superheater	0.149	0.112	0.036	-	0.013	0.019	-	75%
Solution heat exchanger	0.442	0.305	0.136	-	0.051	0.069	-	69%
Subcooler	-	-	0.002	-	0.001	0.001	-	-
Turbine	0.444	0.143	0.300	-	0.111	0.150	-	32%

Fig. 7 shows that both in the simple absorption and CCP configuration, the absorber and the desorber are the components where most of the exergy destruction takes place. For the combined cycle, an important part of the exergy destruction (11.5% in the nominal case) takes place in the turbine. However, as shown in Table 7, the exergetic efficiency of the two configurations in the nominal case are comparable, around 12.2% for the simple absorption configuration and 11.5% for the CCP cycle. As done in the energy analysis, also in the exergy analysis it is interesting to evaluate the performance attainable by an isentropic turbine. In this scenario, the exergetic efficiency of the cycle would double, reaching 24%. This improvement of performance is not reflected in a proportional increase in the η_e which, giving the same value to the cooling and power production, only slightly increases, passing from 0.39 to 0.40.

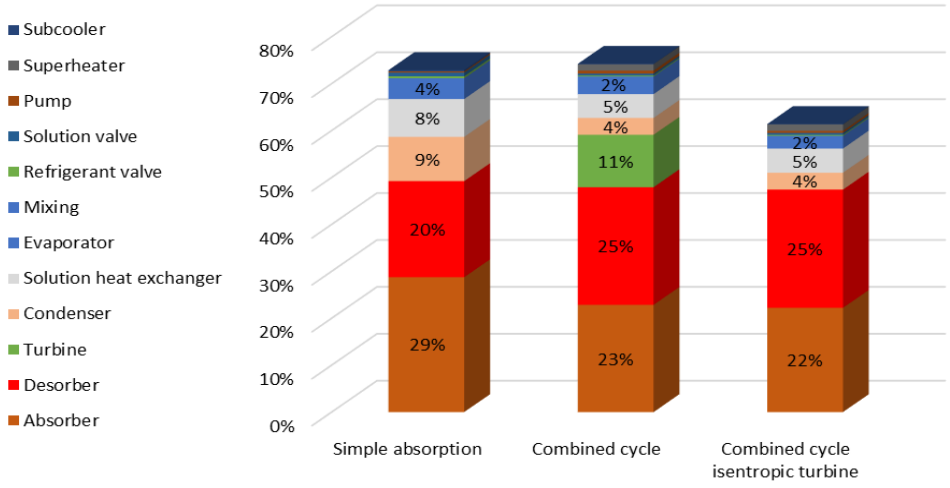

Fig. 7. Non-dimensional exergy destruction ratio ($Y_{D,k}$) of different components in the cycle for the simple absorption and combined configurations.

Table 7. Exergy balance table for the combined cycle configuration at nominal operating conditions.

Configuration	$\dot{E}x_{F,tot}$ [kW]	$\dot{E}x_{P,tot}$ [kW]	$\dot{E}x_{D,tot}$ [kW]	$\dot{E}x_{L,tot}$ [kW]	η_{ex} [%]	η_e [-]	$\eta_{e,id}$ [-]
Absorption cycle only	1.838	0.2255	1.339	0.2731	12.27%	0.684	5.975
Combined cycle	2.693	0.305	1.999	0.305	11.45%	0.389	3.002
Combined cycle isentropic turbine	2.695	0.6633	1.655	0.377	24.30%	0.408	3.002

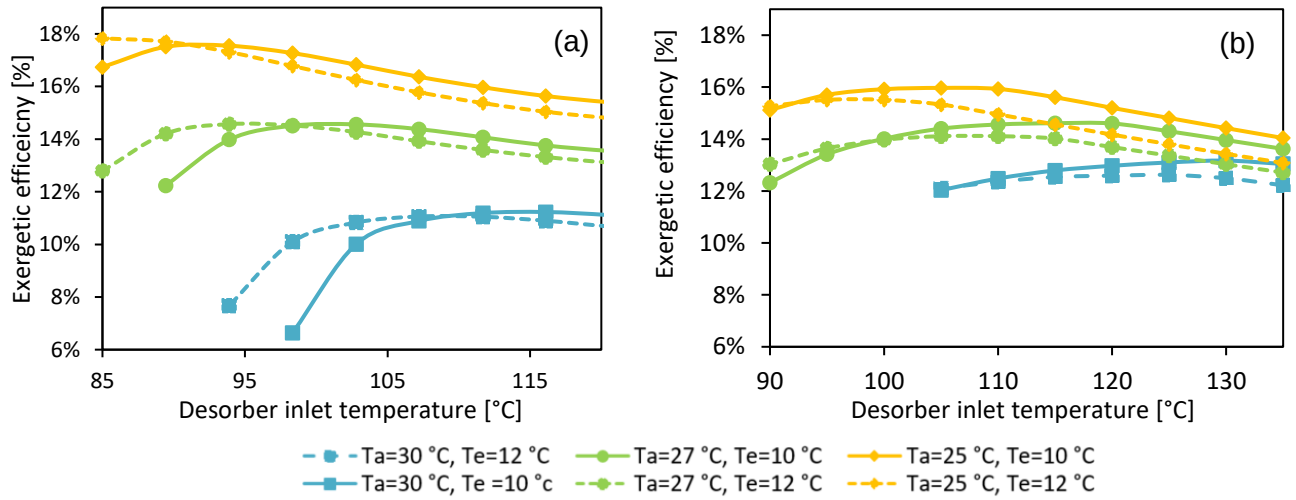

Fig. 8. Influence of the desorber inlet temperature on the exergetic efficiency of the simple absorption (a) and on the CCP cycle (b) configuration.

A parametric analysis on the desorber inlet temperature was performed (Fig 8). All other operating conditions being fixed, there is a desorber inlet temperature maximizing the exergetic efficiency of the cycle. Increasing the intermediate source temperatures reduces considerably the exergetic efficiency of the system in both cases. Comparing Fig. 8(a) and (b), the temperature maximizing the exergetic efficiency increases when passing from the simple absorption to the CCP configuration. The maximum obtainable exergy efficiency for the case of intermediate and cold source temperature of 27 °C and 10 °C respectively is around 14.5% in both cases, despite the low efficiency of the turbine. Fig. 9 shows the exergetic efficiency of the CCP system for sources temperatures variation around the nominal point.

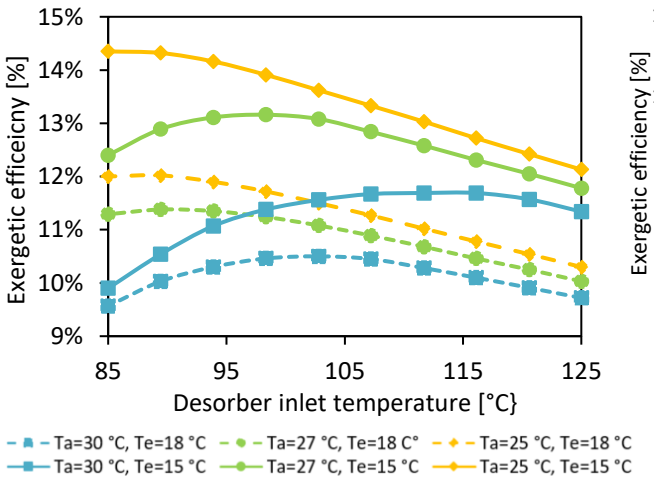

Fig. 9. Influence of the desorber inlet temperature on the exergetic efficiency of the CCP system around the nominal point.

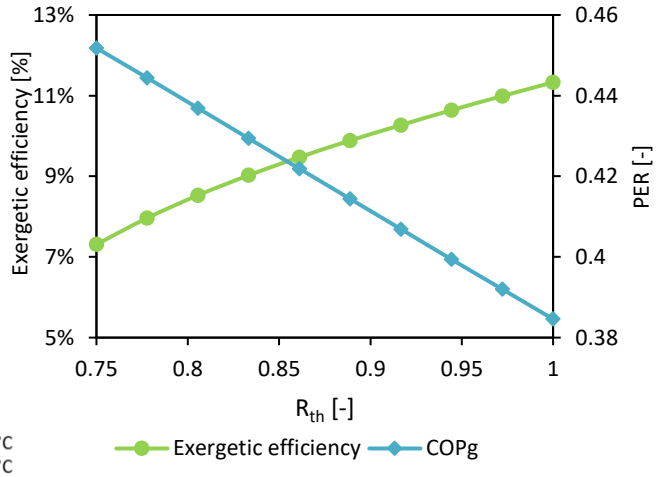

Fig. 10. Influence of the throttling process on the exergetic efficiency

Finally, Fig. 10 shows the effect of the throttling process on the exergetic efficiency of the cycle. It passes from 11.5% to 7% for an R_{th} of 0.75 where the power production of the turbine goes to zero (Fig. 5). On the contrary, since the cooling production increases in absolute value more than the decrease of power production, the η_e of the cycle increases with the throttling process. This highlights again the limits of a purely energy analysis for this kind of combined cycle.

4. Conclusions

Absorption machines represent an alternative to conventional vapour compression systems for their ability to use renewable energy sources and waste heat. The integration of an expander in an absorption chiller is presented in this study as it holds great promise for its ability to harness low-temperature heat sources more efficiently than production with separate cycles.

A model of the turbine tuned on CFD simulations was integrated in a model of the absorption chiller adjusted on experimental measures in order to perform an energy and exergy analysis of the combined cycle. A parameter describing the energy performance of the cycle was introduced and compared to an ideal performance parameter. A parametric analysis on the temperature of the sources was then performed allowing a mapping of the performance of the machine. The study highlights the strict limits imposed by turbine on the cycle in terms of treated mass flow rate, so that the introduction of a throttling process to increase flexibility was assessed. Subsequently, an exergy analysis was performed for both the simple absorption and combined cycle configuration and the components where most of the exergy destruction takes place were identified. It was observed that a hot source temperature maximizing the exergetic efficiency exists for fixed operating conditions.

The analyses developed show the potential of the cycle to produce both power and cooling even at small lab scale and provide reliable insights on the integration of this type of expander in an ammonia-water absorption cycle, pending a scale-up of the technology, expected to increase the efficiency of the system.

Acknowledgments

The authors would like to express their gratitude to the French Alternative Energies and Atomic Energy Commission and the Carnot Energies of the Future Institute. S. Braccio was supported by the CEA NUMERICS program, which has received funding from the European Union's Horizon 2020 research and innovation program under the Marie Sklodowska-Curie grant agreement No 800945.

Appendix A

Table A1. State properties of the streams for the simple absorption configuration at nominal operating conditions.

Stream	T [°C]	P [bar]	h [kJ/kg]	s [kJ/(kg K)]	$\dot{m}$ [kg/h]	x [-]	Physical exergy [kW]	Chemical Exergy [kW]	Total Exergy [kW]
1	33	6.084	-88.7	0.335	100	0.544	0.990	300.9	301.9
2	33.1	12.02	-87.8	0.336	100	0.544	1.011	300.9	301.9
3	64.7	12.02	69.7	0.823	100	0.544	1.352	300.9	302.2
4	85.2	12.02	148.5	1.056	78.46	0.423	0.690	183.7	184.4
5	40.4	12.02	-52.4	0.457	78.46	0.423	0.202	183.7	183.9
6	40.5	6.084	-52.4	0.460	78.46	0.423	0.187	183.7	183.9
7	73.9	12.02	1427	4.682	21.54	0.987	2.097	117.2	119.3
8	73.9	12.02	1427	4.682	21.54	0.987	2.097	117.2	119.3
9	31.4	12.02	139.4	0.530	21.54	0.987	1.803	117.2	119.0
10	16.7	12.02	68.8	0.292	21.54	0.987	1.804	117.2	119.0
11	10.0	6.084	68.8	0.296	21.54	0.987	1.955	117.2	119.1
12	15.0	6.084	1196	4.251	21.54	0.987	1.490	117.2	118.7
13	25.0	6.084	1267	4.491	21.54	0.987	1.484	117.2	118.7

Table A2. State properties of the streams for the combined cycle configuration at nominal operating conditions.

Stream	T [°C]	P [bar]	h [kJ/kg]	s [kJ/(kg K)]	$\dot{m}$ [kg/h]	x [-]	Physical exergy [kW]	Chemical Exergy [kW]	Total Exergy [kW]
1	32.9	6.35	-72.3	0.358	100	0.607	1.634	335.4	337.0
2	34.0	11.71	-71.0	0.360	100	0.607	1.654	335.4	337.1
3	56.2	11.71	77.6	0.822	100	0.607	1.959	335.4	337.4
4	86.2	11.71	154.7	1.072	66.36	0.412	0.571	151.4	152.0
5	36.2	11.71	-69.2	0.401	66.36	0.412	0.129	151.4	151.5
6	36.3	6.35	-69.2	0.403	66.36	0.412	0.118	151.4	151.5
7	65.7	11.71	1401	4.618	33.64	0.992	3.220	184.0	187.2
8	65.7	11.71	1401	4.618	16.2	0.992	1.551	88.6	90.1
9	30.3	11.71	138.1	0.512	16.2	0.992	1.378	88.6	89.9
10	19.0	11.71	83.6	0.329	16.2	0.992	1.378	88.6	89.9
11	11.1	6.35	83.6	0.333	16.2	0.992	1.373	88.6	89.9
12	16.1	6.35	1236	4.359	16.2	0.992	1.155	88.6	89.7
13	26.1	6.35	1290	4.544	16.2	0.992	1.152	88.6	89.7
14	65.7	11.71	1401	4.618	17.44	0.992	1.669	95.4	97.0
15	115.0	11.71	1528	4.968	17.44	0.992	1.782	95.4	97.1
16	95.9	6.35	1498	5.176	17.44	0.992	1.337	95.4	96.7
17	54.4	6.35	1398	4.888	33.64	0.992	2.445	18.0	186.

Nomenclature

Letter symbols

ex	specific exergy, kJ/kg
$\dot{E}x$	exergy, kW
h	specific enthalpy kJ/kg
$\dot{m}$	mass flow rate, kg/s
P	pressure, bar
$\dot{Q}$	thermal power, kW
R	ratio
s	specific entropy, kJ(kg K)
T	temperature, °C
$\dot{W}$	mechanical power, kW
Y	rate of exergy destruction (loss) to total fuel exergy
Y^*	rate of exergy destruction to total exergy destruction
x	ammonia mass fraction

Greek symbols

η	efficiency

Acronyms

CCP	combined cooling and power
COP	coefficient of performance
HTF	heat transfer fluid
ORC	organic Rankine cycle

Subscripts and superscripts

0	reference
1,2,…	system state points
a	absorber
CH	chemical
c	condenser
cv	control volume
d	desorber
D	destroyed
e	evaporator, energy
ex	exergetic
F	fuel
H_2O	water
i	inlet
id	ideal
is	isentropic
KN	kinetic
NH_3	ammonia
o	outlet
P	product
p	pump
PH	physical
PT	potential
Q	thermal
R	refrigeration
s	Split
sh	super-heater
shx	solution heat exchanger
sub	sub- cooler
t	turbine
th	throttling

References

[1] F. Birol, The Future of Cooling-Opportunities for energy efficient air conditioning- Opportunities for energy efficient air conditioning, OECD/IEA 2018. (2018).

[2] A. Godefroy, M. Perier-Muzet, P. Neveu, N. Mazet, Hybrid thermochemical cycles for low-grade heat storage and conversion into cold and/or power, Energy Convers. Manag. 225 (2020) 113347. https://doi.org/10.1016/j.enconman.2020.113347.

[3] S. Braccio, H.T. Phan, N. Tauveron, Study of a cold and electric cogeneration machine using a low temperature heat source., SFT 2021. (2021). https://doi.org/https://doi.org/10.25855/SFT2021-036.

[4] D.S. Ayou, J.C. Bruno, R. Saravanan, A. Coronas, An overview of combined absorption power and cooling cycles, Renew. Sustain. Energy Rev. 21 (2013) 728–748. https://doi.org/10.1016/j.rser.2012.12.068.

[5] F. Boudéhenn, H. Demasles, J. Wyttenbach, X. Jobard, D. Chèze, P. Papillon, Development of a 5 kW cooling capacity ammonia-water absorption chiller for solar cooling applications, Energy Procedia. 30 (2012) 35–43. https://doi.org/10.1016/j.egypro.2012.11.006.

[6] S.A. Ibrahim, O.M., Klein, Thermodynamic properties of ammonia-water mixtures., in: ASHRAE Trans. Symp. 21, 2, 1495, n.d.

[7] S. Braccio, H. Trieu Phan, M. Wirtz, N. Tauveron, N. Le Pierrès, Simulation of an ammonia-water absorption cycle using exchanger effectiveness, Appl. Therm. Eng. (2022) 118712. https://doi.org/https://doi.org/10.1016/j.applthermaleng.2022.118712.

[8] S. Braccio, H.T. Phan, N. Tauveron, N. Le Pierrès, Study of the integration of a supersonic impulse turbine in a NH 3 / H 2 O absorption heat pump for combined cooling and power production from a low temperature heat source , E3S Web Conf. 312 (2021) 08018. https://doi.org/10.1051/e3sconf/202131208018.

[9] M. Puig-Arnavat, J.C. Bruno, A. Coronas, Modeling of trigeneration configurations based on biomass gasification and comparison of performance, Appl. Energy. 114 (2014) 845–856. https://doi.org/10.1016/j.apenergy.2013.09.013.

[10] A. Bejan, G. Tsatsaronis, M.J. Moran, Thermal design and optimization, in: 1995.

[11] A. Vidal, R. Best, R. Rivero, J. Cervantes, Analysis of a combined power and refrigeration cycle by the exergy method, Energy. 31 (2006) 3401–3414. https://doi.org/10.1016/j.energy.2006.03.001.

[12] R.D. Misra, P.K. Sahoo, A. Gupta, Thermoeconomic evaluation and optimization of an aqua-ammonia vapour-absorption refrigeration system, Int. J. Refrig. 29 (2006) 47–59. https://doi.org/10.1016/j.ijrefrig.2005.05.015.

[13] J. Szargut, Exergy method: technical and ecological applications, Int. Ser. Dev. Heat Transf. 18 (2005) 164.

[14] M. Wirtz, Development of a falling-film desorber combining vapor generation and purification for ammonia–water absorption chiller (Modeling and Experiments), PhD Thesis, Université Savoie Mont Blanc, 2022.